Scanning Electron Microscopy

Volume 1986
Number 1 *Part I*

Article 1

1-18-1986

Analytical Ultra High Vacuum Scanning Electron Microscopy with Field Emission Gun for Surface Study

P. Morin
Université Lyon I

P. Abraham
Université Lyon I

C. Bablet
Université Lyon I

M. Tholomier
Université Lyon I

Follow this and additional works at: https://digitalcommons.usu.edu/electron

Part of the Biology Commons

Recommended Citation

Morin, P.; Abraham, P.; Bablet, C.; and Tholomier, M. (1986) "Analytical Ultra High Vacuum Scanning Electron Microscopy with Field Emission Gun for Surface Study," *Scanning Electron Microscopy*: Vol. 1986 : No. 1 , Article 1.
Available at: https://digitalcommons.usu.edu/electron/vol1986/iss1/1

This Article is brought to you for free and open access by the Western Dairy Center at DigitalCommons@USU. It has been accepted for inclusion in Scanning Electron Microscopy by an authorized administrator of DigitalCommons@USU. For more information, please contact digitalcommons@usu.edu.

SCANNING ELECTRON MICROSCOPY/1986/I (Pages 1-9)
SEM Inc., AMF O'Hare (Chicago), IL 60666-0507 USA

0586-5581/86$1.00+05

ANALYTICAL ULTRA HIGH VACUUM SCANNING ELECTRON MICROSCOPY WITH FIELD EMISSION GUN FOR SURFACE STUDY

P. Morin,* P. Abraham, C. Bablet and M. Tholomier

Départment de Physique des Matériaux – Université Lyon I
43 Bd du 11 Novembre 1918, 69622 Villeurbanne – France

(Received for publication January 29, 1985, and in revised form January 18, 1986)

Abstract

Surface studies can be carried out with a scanning electron microscope (SEM) having an ultra high vacuum specimen chamber. The main application of this SEM was the micro Auger analysis, but it is also interesting to combine the usual surface study technique with SEM observations. Indeed, these latter give valuable information about the topographic, chemical and crystallographic aspects of the surface when the secondary, backscattered and transmission SEM modes are used. The SEM performances are increased by the use of a field emission gun, the high brightness beam of this gun gives new observation possibilities such as the imaging of crystallographic defects on solid samples.

Key words: Surface study, micro Auger analysis, ultra high vacuum, scanning electron microscopy, ultra high vacuum SEM, field emission gun, electron backscattered observation, electron secondary observation, scanning transmission electron microscopy, Auger crystalline effect, Auger analysis resolution, channeling observation.

*Address for correspondence:
P. Morin
Départment de Physique des Matériaux
Université Lyon I
43 Bd du 11 Novembre 1918, 69622 Villeurbanne, France
Phone No.: (7) 889-81-24

Introduction

These last years, scanning electron microscopy (SEM) has profited by two important improvements: ultra high vacuum (UHV) specimen chambers allow one to perform surface studies and field emission (FE) guns which give a higher beam brightness and thus allow new possibilities of observation (Christou, 1977; Hembree and Cowley, 1979; Todd et al., 1979; Venables et al., 1980; Ichinokawa et al., 1984). The main interest of UHV-SEM in surface studies is that it allows Auger analysis on small areas with an additional electron-spectrometer. It is also advantageous to combine the usual surface investigations (AES, XPS, UPS, RHEED, LEED . . .) with SEM observations. The specimen must stay in high vacuum. These techniques must then be carried out in situ. The specimen chamber is often not large enough so a supplementary coupled UHV chamber is needed. These chambers must be equipped with specimen preparation facilities e.g., ionic bombardment, specimen heating, fracture attachment, gas introduction device, evaporating system. . . .

The two main technical problems which occur in analytical studies with UHV-FE-SEM are on one hand, design of baking components and on the other hand the field emission stability. We have resolved this problem by heating the tip during emission to avoid the drift of the emission current over a long period, and the residual fluctuations are corrected on the detected signals by dividing these signals by a signal collected on the objective aperture. This solution gives an effective stability better than one per cent. Another method is to stabilize the emission by controlling the extracting voltage applied to the tip driven by the signal aperture. The beam stability is then as low as 0.2 per cent, but the variations of the extractive voltage lead to a defocus in the final spot. Thus this technique can be used only for nonfocus analysis.

List of Abbreviations

AES – Auger electron spectroscopy
BSE – Backscattered electrons
FE – Field emission
FEG – Field emission gun
LEED – Low energy electron diffraction
RHEED – Reflection high energy electron diffraction
SAES – Scanning Auger electron spectroscopy
STEM – Scanning transmission electron microscopy
UHV – Ultra high vacuum
UPS – Ultraviolet photoelectron spectroscopy
XPS – X-ray photoelectron spectroscopy

In the present paper these SEM improvements are demonstrated with surface results from a high energy UHV-FE-SEM (HB 50 A V.G. Ltd.) and a low energy UHV-FE-SEM (designed by the firm ISA-RIBER). Four SEM modes are used:

a) the Auger mode to get chemical information; a field emission gun allows one to reduce the analysed areas

b) the secondary mode, it gives essentially topographic and chemical contrasts; at high resolution the signal to noise ratio of the images is better with a field emission gun

c) the backscattered mode, which gives crystallographic investigations with the electron channeling contrast and the RHEED technique; by use of a field emission gun and by the filtering of the backscattered electrons it is possible to observe individual crystalline defects on solid samples.

d) the transmission mode, though the surface preparations are more difficult with a thin sample, the Auger resolution is improved by suppressing backscattering effect and by using a field emission gun.

Micro Auger mode

The resolution limit of secondary images for a vanishingly small beam current ($\sim 10^{-11}$A, without FE gun) is given by considering only the diffraction and the spherical aberration of the final lens (Wells, 1974a). For the Auger analysis which requires a higher beam current (1-10 nA) the probe diameter depends on the beam brightness, so an SEM with a field emission gun gives smaller probe diameters in this beam current range.

Probe diameter is not the only parameter involved in determining resolution; but it depends on the escape area of the backscattered electrons (Morin, 1985a). Indeed the contribution of the backscattered electrons is not small compared with that of the primary beam. Thus the resolution of the analysis also depends on both the probe energy and the nature of the sample.

It is generally agreed that the square of the probe diameter (d_p^2) is equal to the sum of squares of the aberration diameters with the square of the gaussian diameter. This gives:

$$d_p^2 = 4I \,/\, (\pi^2 \beta_0 \alpha^2 E) + 1/4\, C_S^2 \alpha^6 + (0.6\, \lambda)^2 \,/\, \alpha^2 + C_{ch}\, (e/E)^2\, \alpha^2 \quad (1)$$

where β_0 is the effective brightness at input of the optical system; e is the spread energy of the beam; C_S and C_{ch} are the spherical and chromatic aberration coefficients; λ is the electron wavelength; E is the beam energy. There is an optimum illumination angle (2 α) giving a minimum probe size (Wells, 1974b)

$$d_S^{min} = \{2/27\, R\, (Q^2 + 12\, PR)^{3/2} + Q\, (36\, PR - Q^2)\}^{1/4} \quad (2)$$

with $P = 4/\pi^2\, I/\beta_0\, E^{-1} + 5.4\; 10^{-8}\, E^{-1}$

$Q = (C_{ch} e)^2\, E^{-2}$

$R = 0.25\, C_S^2$

For thermoelectronic or cathode LaB_6 guns, it is the final lens aberrations which are predominant. The beam diameter will be calculated using the aberration coefficients of a magnetic lens focusing the beam from a distance of about 1 cm. For a field emission gun in the case of focusing 1 cm from the final lens, it is the first focusing lens aberrations which are the most important (Fontaine, 1979). Figure 1 gives the minimum probe diameter in terms of electron energy for thermoelectronic cathode LaB_6 and field emission gun. The values of the various parameters for this calculation are given in Table 1. The beam current is taken equal to 10 nA, to obtain an Auger signal with an acceptable signal to noise ratio.

To compare the analysis resolution of various probe forming systems we can suppose that the resolution is given by the expression:

$$D = \sqrt{d_p^2 + d_R^2} \quad (3)$$

where d_R is the escape area diameter of the backscattered electrons; d_R is taken equal to the half of the range R of the electrons (Goldstein, 1975). From Holliday and Sternglass (1959): $R = 0.049/\rho E^{1.65}$ (μm); where ρ is is the volumetric weight (g/cm^3) and E is the beam energy (keV), d_R is given in Figure 1 as a function of beam energy for a copper target (copper having an average density, $\rho = 8.93$ g/cm^3). Figure 1 shows that with a low energy beam, it is probe size which determines analysis resolution, and with a higher beam energy the resolution is given by the escape area of the backscattered electrons.

Thus there is an optimum beam energy giving an optimal analysis resolution in the range of 1 to 10 keV. We have built an electrostatic SEM with a field emission gun composed of a single lens. The focal distance, d_f, is 10 cm (Morin and Simondet, 1984). The probe size as a function of the beam energy has been established experimentally with a beam current of 10 nA, the results give a curve (Fig. 1) which complies with the law

$d_p = 0.37\, E^{-0.7}$

The analysis resolution of this gun can thus be written as above

$D = \sqrt{(0.37\, E^{-0.7})^2 + (0.025/\rho E^{1.65})^2}$

D is minimum for $E_{opt} = 2.7\, \rho^{0.43}$ (keV)

which gives $D_{min} = 0.223\, \rho^{-0.3}$ (μm)

D_{min} and E_{opt} are represented in Fig. 2. The heavier the material the better the resolution (for Au D_{min} = 90 nm with E_{opt} = 10 keV, and for Mg D_{min} = 175 nm with E_{opt} = 3.3 keV).

Electron secondary SEM mode and Auger analysis

The use at the same time of secondary electrons observations by Scanning Electron Microscopy (SEM) and Auger Electron Spectroscopy (AES) is quite interesting. SEM information is almost indispensable to complete those given by AES. This information is essentially intensity variation of the secondary yield due to the topography, the chemical inhomogeneity or the various surface crystallographic orientations of the sample. They permit one to localize and sometimes to identify the analysis area, and also to back up AES information.

The observation of the roughness of a surface sample, in the resolution limit of SEM which is approximately of the magnitude of the electron beam on the surface sample can inform on the validity of the AES measures (Wehbi and Roques-Carmes, 1984). For important rough surface the AES intensity is lowered down to 40% with regard to a relatively smooth surface (Holloway, 1975).

For high resolution Scanning Auger Electron Spectroscopy (SAES), if the beam current intensity is too low (1-10 nA) to have a good Auger signal/noise ratio to plot a chemical mapping of the surface sample, it is possible with SEM to show up

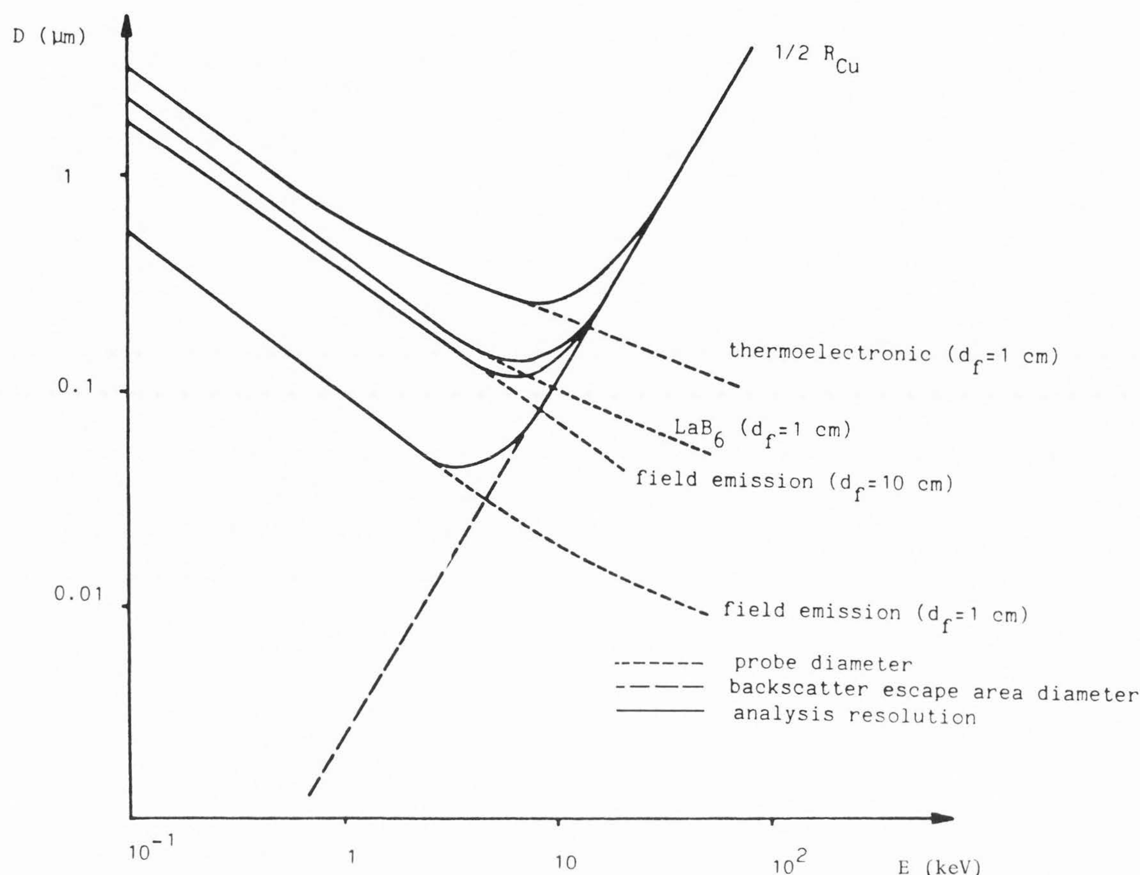

Fig. 1. Auger analysis resolution as a function of electron energy with a 10 nA beam current for various gun types.

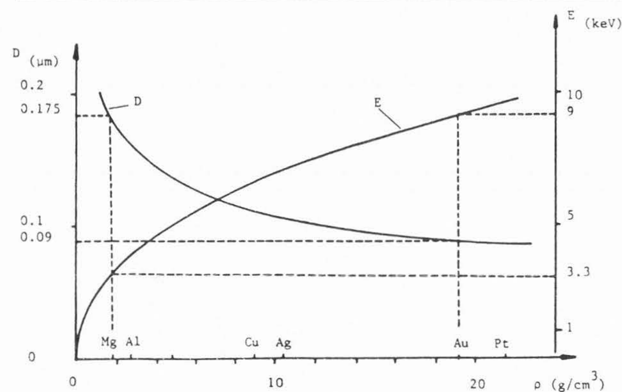

Fig. 2. Optimal analysis resolution (D_{min}) and beam energy in terms of sample density for a field emission gun with a focusing distance of 10 cm.

chemical contrast and then to do localized analysis on the different zones of the samples. This method can also be useful for the analysis of samples sensitive to irradiation damage.

Crystallographic contrast (Boiziau et al., 1983) can also be useful to localize grain boundaries on polycrystalline samples, and then to analyze this area to detect possible segregation or diffusion towards grain boundaries.

Table 1. Values used to calculate d_S (Wells, 1974a)

Gun	I nA	β_o A/(cm^2 Sr keV)	C_s cm	C_{ch} cm	e eV
Th.	10	2 10^3	2	0.8	1.5
LaB_6	10	2 10^4	2	0.8	2.5
F.E.	10	10^7	20	8	0.3

An example of the complementarity of these two techniques is the preparation and then the characterization of the InP(100) surface done in the HB 50 A of Vacuum Generator. It is a high resolution SEM (~ 10 nm) with a field emission gun and AES facilities. After introduction of the sample in the Ultra High Vacuum (UHV) chamber of the SEM, a preparation is required to remove the superficial contaminants (mainly 0 and C). This preparation consists in argon ion sputtering (1 keV, 0.3μA/cm^2) to clean the surface and in annealing to recrystallize the amorphous zone created by argon bombarding. The annealing is carried out with a tungsten heater wire placed under the sample holder, and the temperature is monitored using a platinum/platinum rhodium thermocouple junction soldered on the sample holder. The comparison between the H_P/H_{In} ratio, where H_P and H_{In} are the heights of the phosphorus and indium peaks, measured by linear approximation of the high energy background (Fig. 3) on the N(E) Auger spectra, of this surface and a clean cleaved InP (110) one (which is of stoichiometry 1/2, 1/2), reveals a phosphorus rich surface. Several H_P/H_{In} ratios are given in

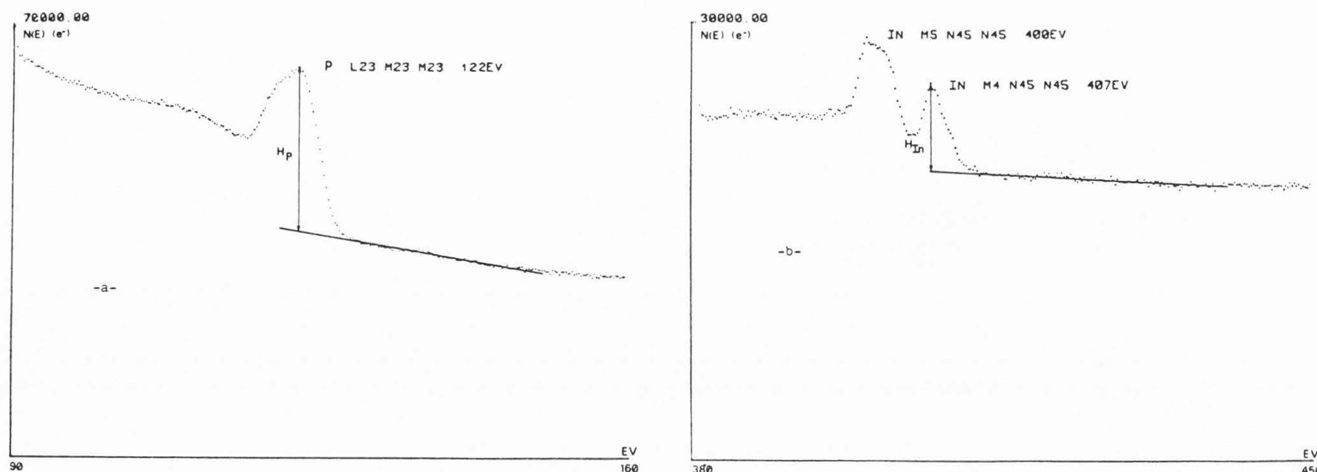

Fig. 3. a) Auger peak of phosphorus on a clean cleaved InP (110) surface **b) Auger peaks of Indium on a clean cleaved InP (110) surface.**

Table 2. H_p/H_{In} ratio for different preparation processes. The InP (100) sample has successively gone through the 5 processes.

Sample	Preparation	H_p/H_{In}
InP(100)	cleavage	4.6
	argon bombarding 1 keV, 0.3 μA cm^{-2}, 3 min.	7.3
	annealing at 150°C 10 min.	6.5
InP(100)	annealing at 200°C 10 min.	6.7
	annealing at 250°C 10 min.	6.4
	annealing at 300°C 10 min.	6.6

Table 2 for different conditions. However the SEM image displays the presence of metallic indium clusters (Fig. 4) of which diameter and surface concentration are respectively about 100 nm and 0.2%. A concentration of such a low magnitude could not have been displayed without the help of SEM. Surface characterization techniques like Auger, UPS, XPS, RHEED . . . are inefficient to resolve this kind of problem, because they are not sensitive enough.

Backscattered electron SEM mode and Auger analysis

The main use of backscattered electrons in SEM is to obtain topographic and chemical contrast. But it is more advisable to use secondary electrons in surface study as resolution is better and analysis depth thinner. Therefore, when selecting low-loss backscattered electrons by energy filtering, the resolution improves so that surface study becomes possible (Wells, 1974c; Christou, 1977).

A more specific use of the backscattered signal is to perform crystallographic observations. The electron channeling patterns give the lattice orientation and the crystalline quality (Pitaval, 1979). For quantitative Auger analysis, the crystallographic orientation is important as in some cases, the channeling effect is responsible for a large change in Auger emission (see e.g. Bishop et al., 1984; Morin, 1985b). The RHEED observations reveal the surface crystallization. The electron channeling imaging is a recent technique to observe crystallographic defects. Together with micro Auger analysis, it should permit determination of the influence of the crystalline defects on the surface properties (Morin et al., 1981).

Auger emission variation induced by channeling effect.

The interactions of the electron beam and emitted electrons with the crystal are responsible for variations of the Auger signal. Three main effects can modify this signal: (i) the anisotropy of the Auger emission, (ii) the diffraction and channeling of the Auger electrons and (iii) the diffraction and channeling of the probe during its penetration in the sample.

Using the rocking beam method in a SEM HB 50 A, it is possible to study only the third effect (Morin 1985b).

The channeling effect occurs when a well collimated beam is tilted near a Bragg position. The beam electrons are either concentrated on the atomic planes or channeled between them in respect to the sign of the angular variation from the Bragg position. When the beam electrons are concentrated on the atomic planes, the backscattered signal increases (Morin, 1983); in the same way, a similar modification of the Auger signal must be expected due to the variation in the rate at which Auger vacancies are created.

The modification of the Auger peak of the Silicon KLL transition is obtained by recording the peak derivative. The variation of the peak to peak height of the peak derivative is plotted in Fig. 5 as a function of the tilt angle; the beam rocks near the axis 100 and describes line A of the electron channeling pattern (Figure 6). The Auger peak varies by a factor greater than 2, the channeling influence is thus considerable in these conditions. It is then indispensable to take into account this effect for any quantitative approach.

Two effects contribute to the variation of the Auger peak: (i) a direct beam effect; the Auger vacancy creation increases or decreases according to whether the electrons are concentrated on the atomic planes or channeled between them, and (ii) an indirect effect, the channeling phenomenon affects the number of Auger electrons created by the backscattered electrons.

A contrast is defined from the maximum and minimum values of the Auger signal (I_{max} and I_{min} respectively) according to the

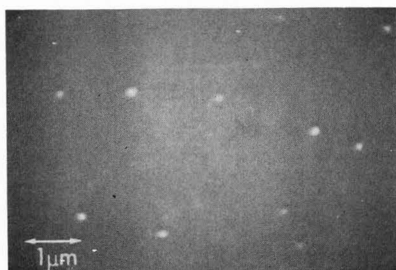

Fig. 4. SEM image of the InP (100) surface after argon bombarding (1 keV, 0.3 μA cm^{-2}, 3 minutes) and successive annealings of 10 minutes at 150, 200, 250 and 300 °C.

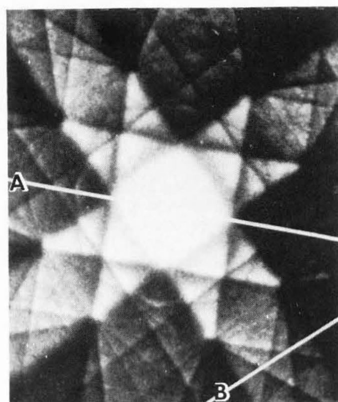

Fig. 6. Electron channelling patterns near the 100 silicon axis.

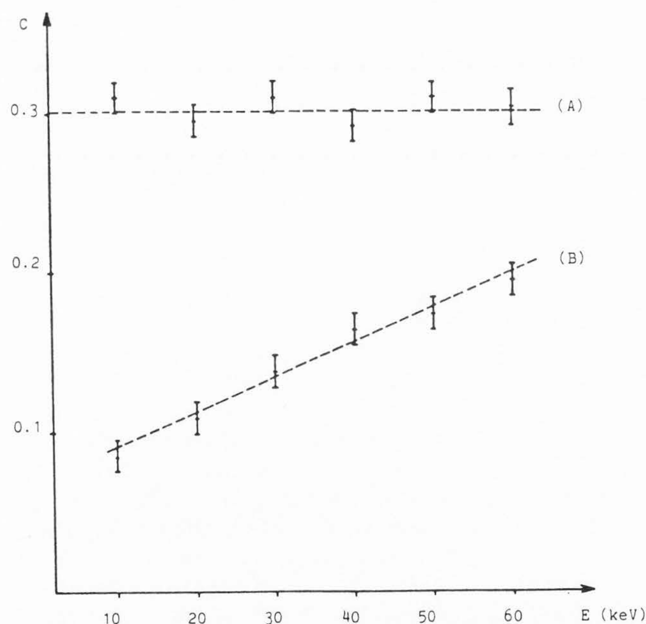

Fig. 7. Contrast of the Auger peak KLL of Si (A) and of background below this peak (B) as a function of the beam energy.

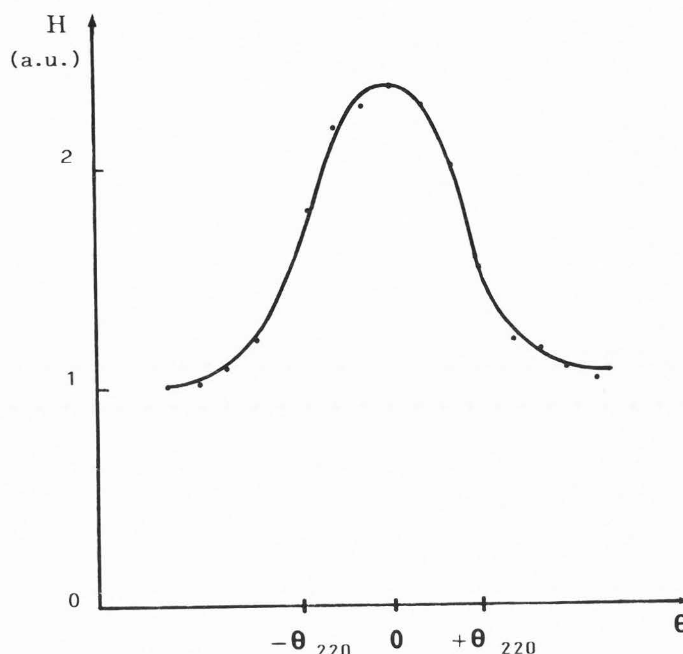

Fig. 5. Silicon KLL Auger peak height as a function of the tilt angle of the beam near the 100 direction.

Table 3. Calculated contrasts of Auger peak KLL and LVV as a function of beam energy.

Beam energy keV	C_{KLL}	C_{LVV}
10	0.71	0.017
20	0.56	0.009
30	0.47	0.0061
40	0.40	0.0047
50	0.36	0.0038
60	0.32	0.0033

channeling state of the beam:

$$C = \frac{I_{max} - I_{min}}{I_{mean}} \quad (4)$$

The contrast of the direct effect has been calculated elsewhere (Morin, 1985b) by the dynamical theory in the two wave approximation:

$$C^j = \mu_g^j / \mu_o^j \, A^2/(1 + A^2) \quad (5)$$
$$\text{with } A = 2\sqrt{2}\, \pi\lambda^j/\xi_g$$

μ_o^j and μ_g^j are the normal and abnormal absorption coefficients of interaction with the shell j electrons.
λ^j is the inelastic mean free path of the Auger electron originated in the ionization of shell j.
ξ_g is the extinction distance.

It has been established (Morin, 1985b) that the ratio μ_g^j / μ_o^j is close to 1 for the silicon core electrons and for the reflection 220. The calculated contrasts due to direct effect, for silicon

KLL and LVV Auger peaks, as a function of beam energy are given in Table 3. The mean free paths of Auger electrons KLL and LVV are taken as equal to 4.8 nm and 0.4 nm respectively (Klasson et al., 1974; Ley et al., 1979). When energy decreases, the channeling of the beam occurs closer to the surface so that more Auger electrons are detected due to their low mean free path, and the contrast is greater.

The contrast of the observed Auger signal is shown in Figure 7 in terms of probe energy. The indirect effect must not be cancelled because the larger part of the Auger electrons is created by backscattered electrons (indirect effect) especially with a high energy probe. The influence of the channeling effect on the backscattering can be shown by measuring the contrast corresponding to the variation of the background under the Auger peaks. This contrast increases with the energy of the probe (Fig. 7) and varies in the opposite way of the contrast due to the direct effect. It is thus possible to explain the observation of a constant contrast in terms of probe energy.

RHEED observations.

In a UHV-SEM, RHEED observations can be obtained by adding a screen in the column axis: the RHEED patterns in Figure 8 exhibit the sub-structure C(4 × 2) on the InP surface (100) after the cleaning process described above. The surface structure is determined with the beam parallel to the 110 (Fig. 8a) and the 100 (Fig. 8b) directions as the RHEED patterns show respectively three and one supplementary lines between the matrix lines.

RHEED patterns with a focus beam on a small area can be obtained due to the high brightness of the field emission gun. According to Figure 9, the beam diameter d on the sample can be expressed as:

$$d \approx \frac{4}{\pi} \frac{1}{\alpha} \sqrt{\frac{I}{\beta}} \tag{6}$$

where Θ is the angular resolution; $\Theta = \frac{D}{L}$ (see Fig. 9)

I is the beam intensity and β is the beam brightness.

In typical conditions ($I = 100$ nA, $\beta = 10^8$ A cm^{-2} sr^{-1}, $\alpha = 10^{-3}$ rad, for $E_{beam} = 30$ keV) the beam diameter has a value of 0.4 μm with a specimen tilt angle of 89°. The analyzed area is quite a rectangle, 23 μm long and 0.4 μm wide. With a thermoelectronic gun, the corresponding area would be 10^3 times larger.

Electron channeling imaging of crystalline defects.

Images of extended crystalline defects beneath the surface of solid samples can be observed when using the low loss backscattered electron signal (Morin et al., 1979, 1981). When a beam of constant incidence in Bragg position scans an imperfect crystal (containing an edge dislocation for example) a channeling contrast appears due to the bending of lattice planes near the dislocation core which modifies the diffracting conditions of the beam. Thus we must expect the same contrast as in the electron channeling patterns situation, where the beam diffracting conditions are modified by the rocking beam method. However, to observe such a contrast, the beam must conform to certain conditions (beam diameter ~10 nm, illumination angle 1.5 10^{-2} rad, beam intensity ~20 nA). So a high brightness is needed (1.4 10^8 A cm^{-2} sterad^{-1}). Such a high brightness requires a field emission gun. This technique has been carried out in an ultra high vacuum scanning microscope (V.G. HB 50 A). A high voltage half-cylindrical mirror analyser was used to filter backscattered electrons up to 60 keV. Figure 10 exhibits edges dislocations on a solid sample of silicon.

Transmission SEM mode and Auger analysis

Thin film or thin foil Auger analysis is the straightforward method to reduce the backscattered electron (BSE) effects. The first experiments were carried out by Wiedmann and Seiler (1977); Wittry (1980) suggested the use of thin films to improve the minimum mass detection limit. Furthermore the field emission gun permits improved sensitivity with thin samples since the detected volume percent varies as $I/\sqrt{\beta}$ (β: brightness of the source). The elimination of BSE effects results in a decrease of Auger peak intensity which is approximately compensated by the background reduction.

To detect an Auger peak of low intensity, it is necessary to know the Auger peak height to background ratio (P_A/B) variation as a function of the primary energy. This permits one to optimize the primary energy range for Auger electron excitation. Furthermore, the Auger peak height must be three times greater than the root mean square fluctuations in background. Figure 11 gives the P_A/B) variation as a function of the primary energy for the 351–356 eV $M_{4,5}$ VV Auger transitions of a 70 nm silver thin film. It must be noticed that optimizing the P_A/B) ratio requires primary energies higher than 7.5 keV, i.e., $U = Ep/Ei < 20$. The (P_A/B) ratio is somewhat lower for thin films than for bulk specimens: this comes from the generation efficiency difference in Auger electron and secondary electron emission. For high energy primary electrons, the ionization cross-section of Auger electrons is more important than the secondary emission cross-section and consequently the bulk sample (P_A/B) ratio is higher (Tholomier, 1986).

Thin film Auger analysis eliminates the tail of the BSE distribution: so the spatial resolution is improved. This tail is particularly important for low Z materials (nearly 2 × 20 μm at 50 keV for silicon with normal incidence). It results in a matrix characteristic Auger peak for localized analysis of islands on a substrate. Generally speaking, it may produce parasitic peaks which disturb the chemical analysis interpretation of the localized defect. Experimental measures of spatial resolution for thin film Auger analysis are very difficult. It requires a check sample with a step like chemical boundary. The "discontinuity width" must be lower than the spot size of the field emission gun if not, a broadening effect is produced due to the convolution of spot size and discontinuity width. When the used signal results from the backward emitted Auger electrons (reflected Auger signal) the broadening of the incident beam comes mainly from inelastic scattering by single-electron excitation. The corresponding impact parameter p may be determined by:

$$p \approx \frac{vh}{\Delta E} \tag{7}$$

(ΔE energy loss of the ionizing incident electron, v velocity of the incident electron). For the 350 eV $M_{4,5}$VV Auger line excited by a 50 keV primary electron beam, this broadening is near 0.75 nm, thus it is small in respect with the beam diameter (~10 nm). The broadening by elastic scattering of the incident beam inside the sample does not matter for the reflected Auger signal.

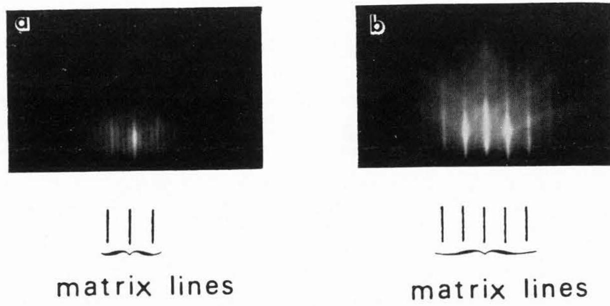

Fig. 8. RHEED patterns on an InP 100 surface
a) beam // 110
b) beam // 100

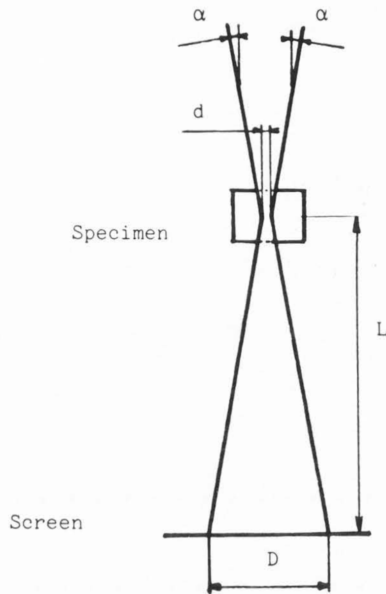

Fig. 9. Focus RHEED pattern conditions.

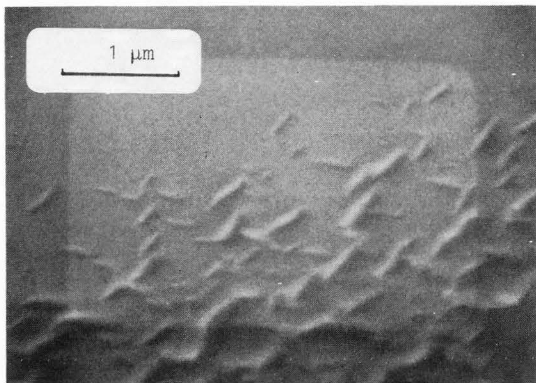

Fig. 10. Edge dislocations on a solid sample of silicon.

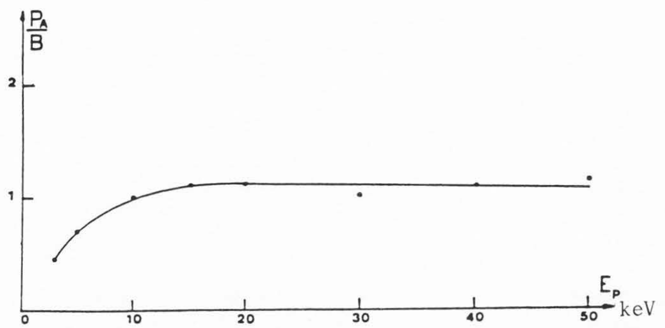

Fig. 11. Auger peak height to background ratio in terms of primary energy for a 70 nm silver thin film (350 eV, $M_{4,5}VV$ Auger transition).

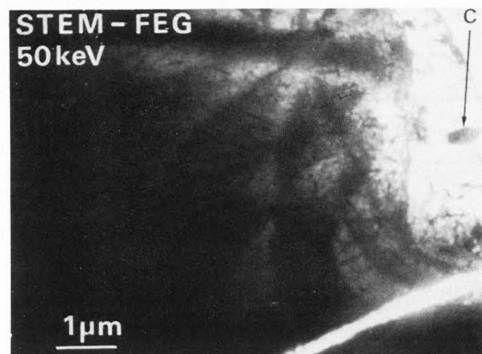

Fig. 12a. Disc-shaped precipitates of chromium in a copper matrix STEM micrograph (bright field).

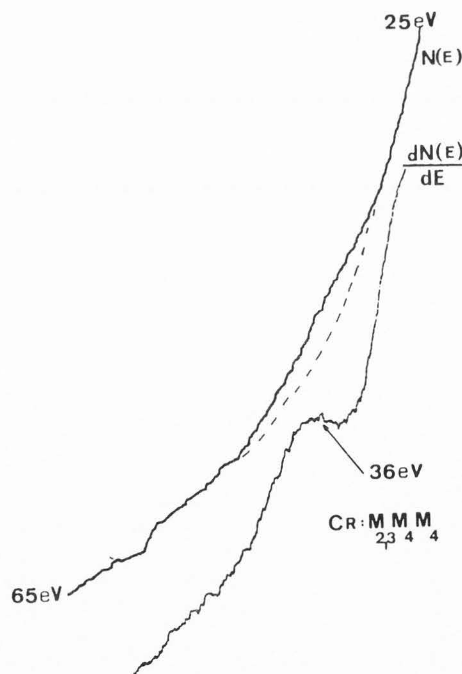

Fig. 12b. Chemical analysis of the precipitate: chromium is identified by the 36 eV $M_{2,3}M_4M_4$ transition.

Applications of thin films Auger analysis come from the ability to correlate STEM observations and chemical analysis of localized defects. The STEM furnishes image with good spatial resolution and permits one to identify the crystalline nature of the observed defects with conventional methods (bright field/dark field). Auger analysis permits one to determine the chemical nature of the defects without matrix influence. The STEM micrograph (Figure 12a) shows disc-shaped precipitates in a Cr/Cu alloy with 0.6% chromium weight. Simultaneous observations by SEM and STEM are possible. Chemical analysis was realized on the C precipitate which is normal to the direction of the incident beam: corresponding N(E) and dN(E)/dE spectra on the precipitate and out of the precipitate are shown in Fig. 12b (Tholomier, 1986).

The use of FEG with high energy probes will permit an interesting development of thin film Auger analysis.

Conclusions

It has been found that the surface properties of materials depend on their topographic aspect, chemical nature, crystallographic state. Thus for non-homogeneous samples a local characterization is necessary. The various surface aspects can be investigated with good resolution by a UHV-FE-SEM with the help of its observation modes (Auger, secondary, backscattered, transmission. . .). The tendency is then to carry out the surface experiments by connecting the usual surface techniques around the UHV-FE-SEM.

References

Bishop HE, Chornick B, Le Gressus C, Le Moel A. (1984). Crystalline effects in Auger Electron Spectroscopy. Surface and Interface Analysis, **6**, No. 3: 116–128.

Boiziau C, Duraud CP, Le Gressus C, Massignon C. (1983). Ultra High Vacuum Analytical Electron Microscopy: an interpretable secondary electron image for Surface Science, Scanning Electron Microsc. 1983; IV: 1525–1534.

Christou A. (1977). Correlation of low loss electron images with Auger images of semiconductor substrate surface. Scanning Electron Microsc. 1977; I: 159–166

Fontaine G. (1979). Microanalysis and Scanning Electron Microscopy. F. Maurice, L. Meny, R. Tixier (Eds.), Les Editions de Physique Orsay France, 13–33.

Goldstein JI. (1975). Practical Scanning Electron Microscopy. Goldstein JI, Yakowitz H. (Eds.), Plenum Press, New York and London, Chap. 1.

Hembree GG, Cowley JM. (1979). Electron channeling and microdiffraction from crystal surface. Scanning Electron Microsc. 1979; I: 145–152.

Holliday JE, Sternglass EJ. (1959). New method for range measurements of low-energy electrons in solids. J. Appl. Phys.; **30**, 1428–1431.

Holloway PH. (1975). The effect of surface roughness on Auger Electron Spectroscopy. J. Electron Spectrosc. and Related Phenom., **7**, 215–232.

Ichinokawa T, Ampo H, Kinoshita S. (1984). Analytical low voltage SEM in UHV for solid surface. Journal de Physique supplément au No. 2, **C2-45**, 301–306.

Klasson M, Berdtson A, Hedman J, Nilsson R, Nyholm R, Nordling C, Cardona DM. (1974). Electron escape depth in silicon. J. Electron. Spectrosc. **3**, 427.

Ley L, Cardona M, Pollak RA. (1979). Photoemission in solids. L. Ley, DM Cardona (Eds.), Springer Verlag, Berlin, T2 vol. **27**, 11–172.

Morin P. (1983). Interactions electrons rapides-matières: canalisation électronique. Le Vide, Les Couches Minces, **215**: 105–115.

Morin P. (1985a). Resolution by Auger Micro Analysis. J. Electr. Spectrosc. & Related Phenomen. **37**, 171–179.

Morin P. (1985b). Crystalline effects on Auger emission; the influence of the electron channeling of the probe in scanning Auger microscopy, Surface Sci., **164**, 127–138.

Morin P, Simondet F. (1984). Canon à émission de champ pour microanalyse spectroscopie d'électrons Auger. Journal de Physique supplément au No. 2; **C2-45**, 307–308.

Morin P, Pitaval M, Besnard D, Fontaine G. (1979). Electron channeling imaging and scanning electron microscopy, Phil. Mag A, **40**, 4:511–524.

Morin P, Pitaval M, Tholomier M, Fontaine G. (1981). Electron channeling imaging of defects in PN junction in semiconductor devices and correlation with EBIC images. J. Microsc. Spectrosc. Electron., **6**, 257–265.

Pitaval M. (1979). Microanalysis and Scanning Electron Microscopy, F. Maurice, L. Meny, R. Tixier (Eds.), Les Editions de Physique, Orsay, France, 391–404.

Tholomier M. (1986). Thin films Auger analysis, Journal of Applied Physics, in press.

Todd G, Poppa H, Veneklasen LH. (1979). Auger electron spectroscopy applications of a new integral field emission gun with a small spot size. Thin Solid films, **57**, 213–219.

Venables JA, Janssen AP, Akhter P, Derrien J, Harland CJ. (1980). Surface studies in UHV field emission gun scanning electron microscope. Journal of Microscopy, **118,3**, 315–365.

Wehbi D, Roques-Carmes C. (1984). The effect of surface roughness on Auger Electron Spectroscopy, J. of Applied Physic, **45**, c-2, 319–322.

Wells OC. (1974a). Scanning Electron Microscopy, McGraw-Hill, New York, chap. 4, 81.

Wells OC. (1974b). Scanning Electron Microscopy, McGraw-Hill, New York, chap. 4, 80.

Wells OC. (1974c). Scanning Electron Microscopy, McGraw-Hill, New York, chap. 6.

Wiedmann P, Seiler H. (1977).Ein Einfaches UHV Transmission-Raster Augerelektronen Mikroscop, Optik, **49**, No. 3, 295–300.

Wittry DB. (1980). Spectroscopy in microscopy and microanalysis; the search for an ultimate analytical technique, 7th Euro. Cong. on Elec. Microsc. Foundation, P. Braderno and V.E. Coslette (Eds.), Hague, The Netherlands, Vol. 3, 14–21.

Discussion with Reviewers

J.M. Cowley: On the assumption that your Figure 6 was obtained with secondary or backscattered electrons, it appears from Figure 5 that an Auger channeling pattern would have much poorer angular resolution. Why should this be so?
Authors: Figure 6 was obtained with backscattered electrons and the corresponding Auger channeling pattern has poorer angular resolution. The contrast interpretation is not easy. We must take into account a lot of waves in dynamical theory due to this crystallographic orientation and a thinner crystal layer concerned by the Auger emission.